Guided-Wave Characteristics of Periodic Coplanar Waveguides With Inductive Loading—Unit-Length Transmission Parameters

Lei Zhu, *Senior Member, IEEE*

***Abstract*—Periodic coplanar waveguides (CPWs) with inductive loading are thoroughly studied with resorting to unit-length transmission parameters, i.e., propagation constant and characteristic impedance, of an equivalent dispersive and/or lossy transmission line. The admittance-type method of moments (MoM) is at first formulated to full-wave modeling of a finite-cell periodic CPW with the two feeding lines and then the short-open-calibration procedure is carried out to deembed the two-port $ABCD$ matrix of the core periodic CPW section. Thus, the above two parameters can be extracted from the MoM simulation to exhibit their guided-wave characteristics, i.e., slow-wave and bandstop behaviors. It is for the first time demonstrated that within the bandstop or bandgap, the propagation constant must become complex with a nonzero attenuation constant, while the characteristic impedance appears purely imaginary. Three periodic CPW circuits with six finite cells are then characterized on a basis of the transmission-line theorem and the derived S-parameters are validated by Momentum simulation and RF measurement.**

***Index Terms*—Bandstop, characteristic impedance, inductive loading, method of moments (MoM), periodic coplanar waveguide (CPW), propagation constant, short-open calibration (SOC), slow wave.**

I. Introduction

SINCE THE so-called photonic bandgap (PBG) microstrip line was introduced in [1], it had attracted a tremendously increasing interest in developing various PBG structures for high-performance microwave circuits [2] by utilizing their wide frequency range of rejection, i.e., bandgap or bandstop. Thus far, extensive research has been conducted to demonstrate such an attractive bandstop behavior of planar PBG transmission-line structures with different configurations of the PBG cell by resorting to the resultant scattering matrix of a two-port device. As emphasized in [3] and [4], the PBG structures are, in fact, the alternative terminology of planar transmission lines with inductive loading at a periodic interval. Thus, it is critically preferred to study these periodic structures in terms of unit-length transmission parameters, i.e., propagation constant and characteristic impedance, of an equivalent uniform transmission line, as discussed in much of the early literature, e.g., [5].

To deal with the ideal infinite-periodic structure, the Floquet's theorem was often used to transform a complicated three-dimensional (3-D) problem into its simple two-dimensional (2-D) counterpart under certain restrictive assumption. Using the 2-D method of moments (MoM), the phase constant and real characteristic impedance of periodic microstrip lines were calculated in [6] and [7], and they were initially exhibited to sharply vary with frequency outside the bandstop range. In [8], the matrix pencil technique was applied in the 3-D source-type MoM to directly deembed the real quantities of two such parameters at low frequency for a finite-periodic microstrip line. Recently, this technique was extended in [9] to investigate the frequency-dependent phase constant within the bandstop range. However, no research has been really done so far to investigate the entire guided-wave characteristics of planar periodic structures with resorting to unit-length transmission parameters rather than the S-matrix of the overall finite-periodic circuit blocks.

In the past years, a so-called short-open calibration (SOC) procedure [10] was developed in the admittance-type MoM to effective deembedding of a variety of lumped-element planar circuits (e.g., [10] and [11]) and 3-D definition of characteristic impedance of planar transmission lines [12]–[15]. This MoM–SOC technique is applied here to investigate a variety of periodic coplanar waveguides (CPWs) with inductive loading [16], [17] via extracted unit-length transmission parameters. At first, a brief description is made of the MoM–SOC modeling of periodic CPW structures with finite cells. Extensive results are then provided to exhibit their basic guided-wave characteristics such as slow-wave and bandstop behaviors. Finally, an S-matrix of three six-cell periodic CPW circuits are calculated on a basis of a simple transmission-line theorem in comparison to those obtained from the Momentum simulator and RF measurement.

II. MoM–SOC Modeling Technique

Fig. 1(a) indicates the physical layout for MoM–SOC modeling of a generalized periodic CPW structure with finite cells (N), which are driven by the two CPW feeding lines. In order to establish the source-type magnetic-field integral equation [18], the two impressed current sources I_{S1} and I_{S2} are simultaneously introduced at the two ports. As such, the unknown electric field over the slot area can be numerically solved based on the Galerkin's technique, thus deriving the relationship between the two sets of port currents and voltages, as described in [10] and [11]. The two port locations are selected far away from the two reference planes in Fig. 1(a), i.e., P_1 and P_2, in order that all the high-order modes excited by nonideal current sources vanish at

Manuscript received March 6, 2003; revised May 15, 2003.

The author is with the School of Electrical and Electronic Engineering, Nanyang Technological University, Singapore 639798, Singapore (e-mail: ezhul@ntu.edu.sg).

Digital Object Identifier 10.1109/TMTT.2003.817435

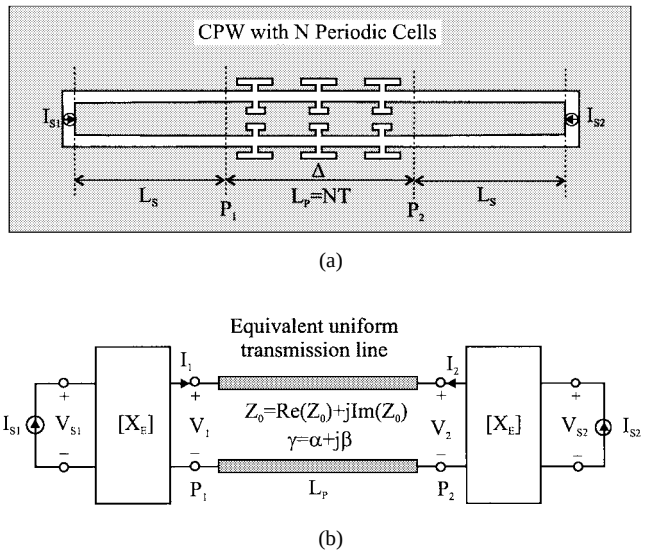

Fig. 1. Physical layout and equivalent-circuit network for MoM–SOC modeling of a periodic CPW structure with inductive-loaded finite cells (N). (a) Physical layout. (b) Equivalent-circuit network.

the two reference planes of our concern. In other words, only the excited dominant quasi-TEM mode can reach these two references. For this reason, the whole layout is classified into the two distinct parts [10]: the core finite-cell periodic CPW section and two CPW feeding lines, which are cascaded via the dominant CPW mode. Fig. 1(b) depicts its relevant equivalent-circuit network in which the periodic CPW is equivalently perceived as the uniform dispersive and lossy transmission line [5]. The two error boxes indicate the electrical behavior of the two source-driven feeding lines, including all the dynamic discontinuity effects caused by the nonideal impressed sources [10].

The SOC technique is then employed in the consistent MoM to independently characterize these error boxes via two calibration standards, i.e., CPW short- and open-end elements, as detailed in [10] and [11] for the microstrip-line case. These two standards are realized here by terminating the reference plane of each CPW feeding line with vertical electric and magnetic walls in the MoM, respectively, thereby equivalently constructing the ideal CPW short- and open-end circuits [15], [18]. In this way, the network parameters of these error boxes can be modeled in terms of the MoM-calculated equivalent voltages at the port and reference in relation to the impressed current at the port. By calibrating them out of the overall network at the two ports, the core network of the central transmission line can be extracted in a straightforward way via the cascaded topology in Fig. 1(b). Thus, complex characteristic impedance ($Z_0 = \mathrm{Re}(Z_0) + j\mathrm{Im}(Z_0)$) and propagation constant ($\gamma = j\beta + \alpha$) of such a uniform periodic CPW with a finite length of $L_p = NT$ can be explicitly calculated in terms of the above-derived $ABCD$-matrix with the elements A_p, B_p, C_p, and D_p as follows:

$$Z_0 = \sqrt{\frac{B_p}{C_p}} \tag{1}$$

$$\cosh(\gamma L_p) = \frac{A_p + D_p}{2} \tag{2}$$

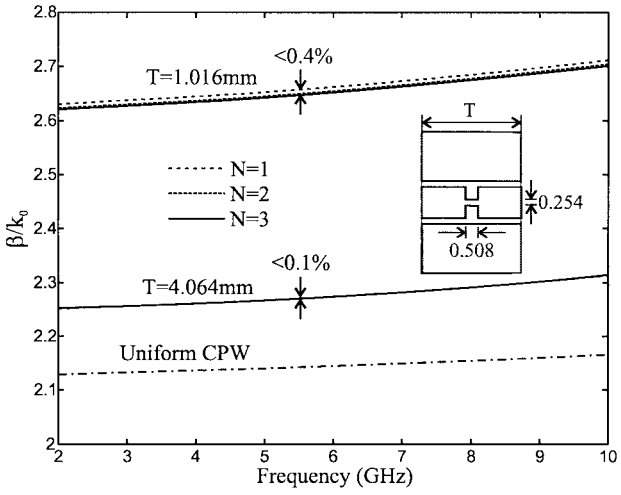

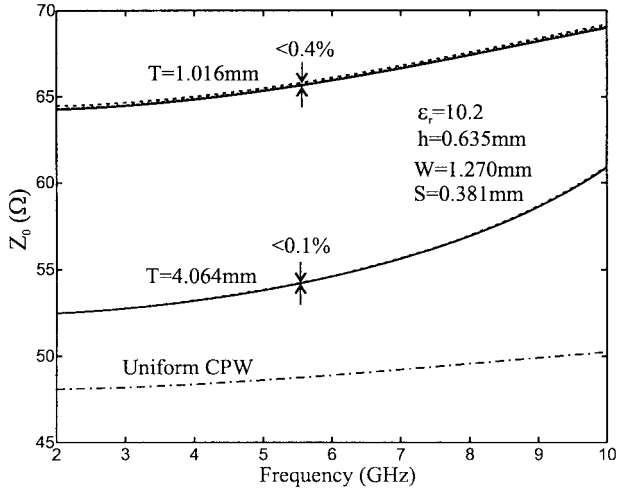

Fig. 2. Extracted unit-length transmission parameters of the periodic CPW structure with $T = 1.016$ and 4.064 mm under the finite cells of $N = 1, 2, 3$. (a) Normalized phase constant. (b) Characteristic impedance.

III. Extracted Results and Validation

Based on the above-described MoM–SOC technique, a variety of periodic CPW structures with different inductive loadings, including the uniform CPW, can be numerically characterized, and their guided-wave performance can be investigated in terms of unit-length transmission parameters. Fig. 2(a) and (b) depicts the calculated phase constant and characteristic impedance of a finite-cell periodic CPW structure with the periodicity of $T = 4.064$ and 1.016 mm, respectively. This structure was originated in [16] to construct the miniaturized CPW resonator by narrowing a small portion of the central conductor in each periodic cell. From Fig. 2(a), the normalized phase constant (β/k_0) is observed to quickly shift up from 2.13, 2.26, to 2.63 as T is reduced from infinity (uniform CPW), 4.064–1.016 mm, thereby exhibiting that the slow-wave behavior of the guided-wave propagation velocity is reduced. Meanwhile, the characteristic impedance (Z_0) rises up from 48.0, 52.6, to 69.0 Ω at the low frequency (2.0 GHz),

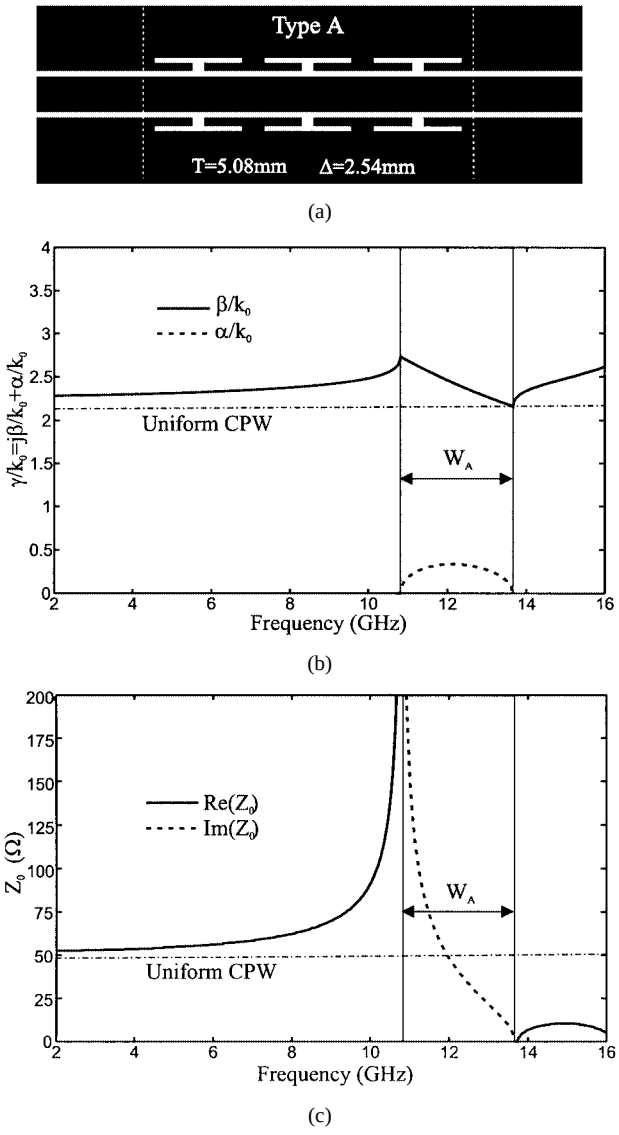

Fig. 3. Geometry and extracted unit-length transmission parameters of the periodic CPW: Type (A). (a) Layout. (b) Normalized propagation constant. (c) Characteristic impedance.

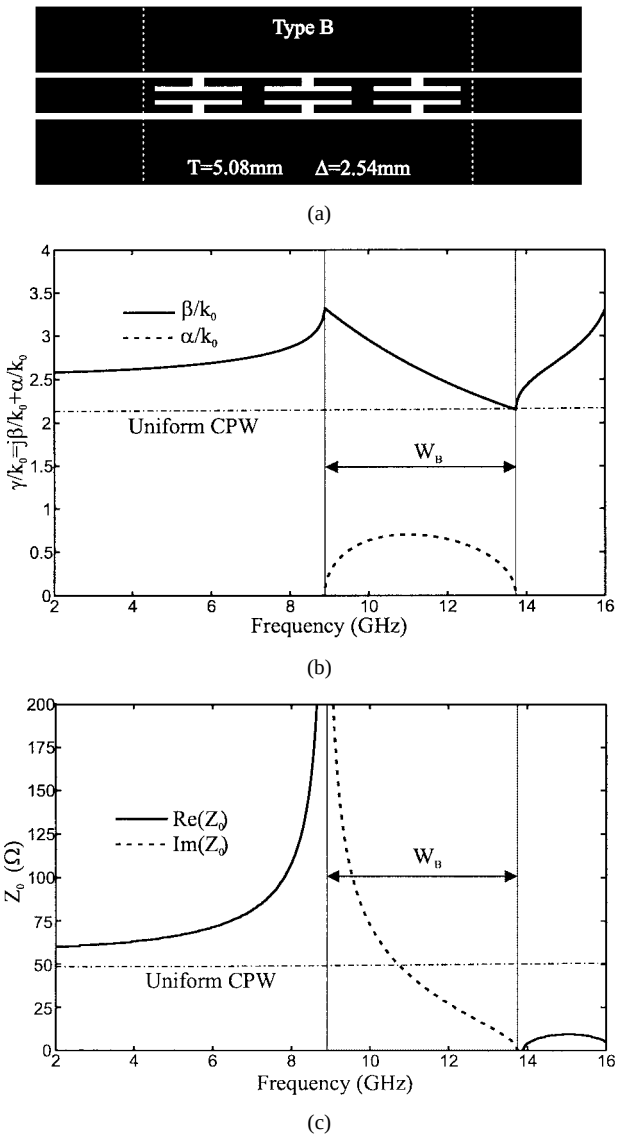

Fig. 4. Geometry and extracted unit-length transmission parameters of the periodic CPW: Type (B). (a) Layout. (b) Normalized propagation constant. (c) Characteristic impedance.

as shown in Fig. 2(b). To ensure the numerical convergence with respect to the finite cells (N) in modeling, three sets of extracted parameters are plotted together in Fig. 2(a) and (b), and the discrepancies among them are found intolerably small with the error below 0.4%. Further, the slight increment of β/k_0 and Z_0 with frequency demonstrates their frequency-dispersive characteristic, as also existed in the uniform CPW [15].

Our special attention is now focused on the investigation of the guided-wave bandgap or bandstop characteristic of periodic CPW structures with enhanced inductive loading. As illustrated in Figs. 3(a), 4(a), and 5(a), they are formed by expanding a pair of transverse slots on the ground plane and/or on the signal conductor, and then they are crouched in parallel to the CPW line in order to keep the low radiation loss.

Figs. 3(b), 4(b), and 5(b) depict the extracted complex propagation constant of these three CPW with fixed periodicity ($T = 5.08$ mm) and slot dimension ($\Delta = 2.54$ mm) against that of the uniform CPW. At first, only the real phase constants (β/k_0) can be observed at low frequency, in which Type C achieves the largest slow-wave factor. Secondly, they tend to increment slowly and then quickly to their relevant maximum values as frequency increases for all three periodic CPW structures. Afterwards, all the β/k_0 fall down with frequency, while the imaginary attenuation constant (α/k_0) comes out, goes up and down, and then disappears. In fact, the band range with nonzero α/k_0, as shaded in Fig. 3(b), 4(b), and 5(b), is referred to as the so-called bandgap or bandstop, as in [5], because of its wave attenuation or rejection behavior. Moreover, it can be seen that these three structures have different bandstop widths, i.e., $W_A = 1.42$ GHz (Type A), $W_B = 2.41$ GHz (Type B), and $W_C = 2.77$ GHz (Type C), exhibiting that Type C with both paired slots on the ground and strip conductor achieves the widest bandstop width.

Figs. 3(c), 4(c), and 5(c) describe the extracted complex characteristic impedance with real and imaginary parts, i.e., $\mathrm{Re}(Z_0)$ and $\mathrm{Im}(Z_0)$, of the three CPW structures discussed above. At

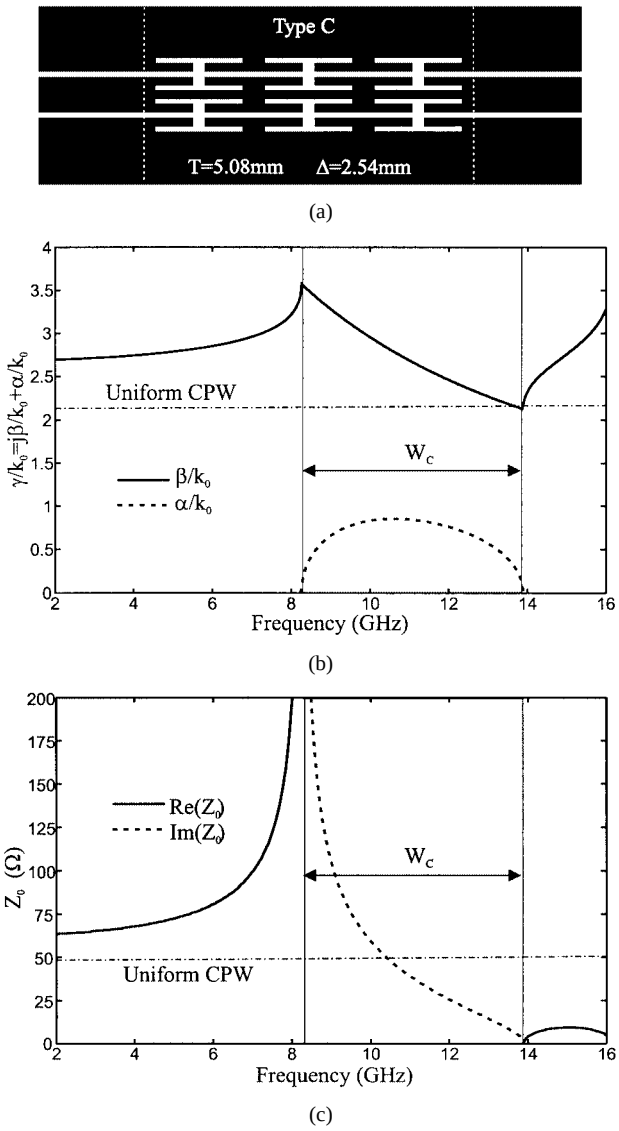

Fig. 5. Geometry and extracted unit-length transmission parameters of the periodic CPW: Type (C). (a) Layout. (b) Normalized propagation constant. (c) Characteristic impedance.

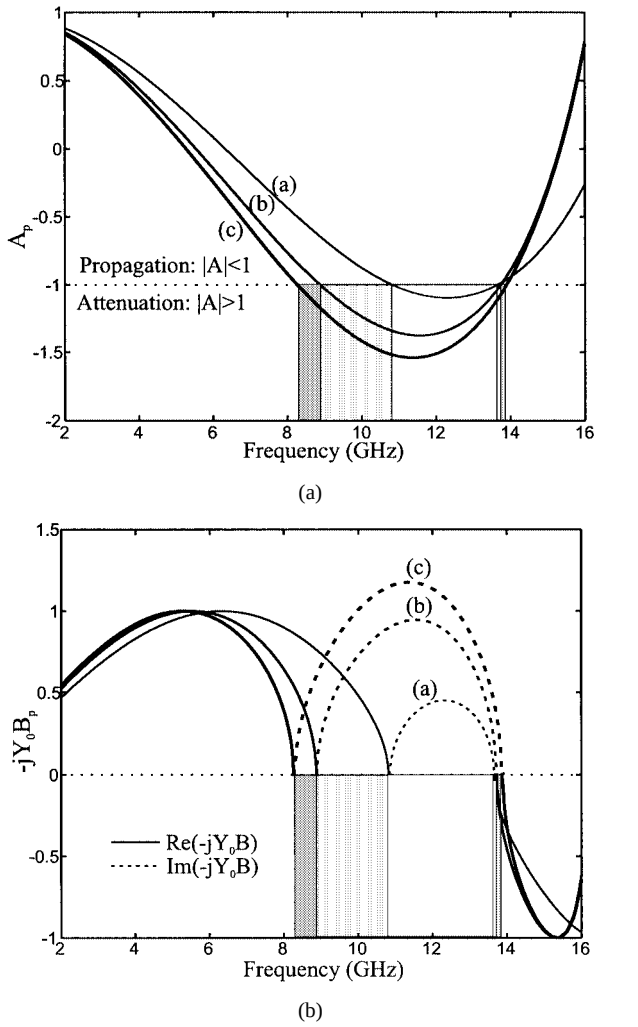

Fig. 6. Calculated $ABCD$-matrix parameters of three types of periodic CPW structures with a single periodic cell for physical explanation on the bandstop behavior, as in Fig. 3–5. (a) A element. (b) B element.

the low-frequency range, $\mathrm{Re}(Z_0)$ starts to rises up slowly and then in an exponential way to infinity, while $\mathrm{Im}(Z_0)$ is kept to zero. As frequency is raised into the bandstop, $\mathrm{Re}(Z_0)$ suddenly disappears to be converted to its infinity imaginary counterpart, i.e., $\mathrm{Im}(Z_0)$, and then $\mathrm{Im}(Z_0)$ drops off very quickly to zero. Beyond the bandstop, $\mathrm{Im}(Z_0)$ is converted again to $\mathrm{Re}(Z_0)$ with small quantity. Herein, the nonzero $\mathrm{Im}(Z_0)$ within the bandstop gives an alternative physical view on the guided-wave bandstop of periodic CPW structures.

To explain the above results, the $ABCD$-matrix parameters of the single-cell periodic CPW structures are obtained via the MOM–SOC and the relevant results are plotted in Fig. 6. Fig. 6(a) shows us that, as frequency increases, A_p starts to fall down from the positive value $(< +1)$ to -1 at the lower edge of the bandstop discussed above, then becomes less than -1 within the overall bandstop, and finally rises up again above -1. Based on the expanded expression of $A_p = \cos(\beta - j\alpha)T$ in (3), we can understand that α must be zero in the range of $-1 \leq A_p \leq +1$, while in the range of $A_p \leq -1$, α must be nonzero and β must be satisfied with the condition of $\beta T = \pi$. Thus, it intuitively confirms the results in Fig. 3(b), 4(b), and 5(b) and also implies that β must drop off as the function of $1/f$, where f is the frequency within the bandstop as follows:

$$A_p = \frac{e^{\alpha T} + e^{-\alpha T}}{2}\cos(\beta T) + j\frac{e^{\alpha T} - e^{-\alpha T}}{2}\sin(\beta T). \quad (3)$$

On the other hand, the calculated B_p is always kept purely imaginary over a whole frequency range. Herein, an alternative B_p-related parameter $-jY_0B_p = \sin(\beta - j\alpha)T$ is defined and Fig. 6(b) depicts its relevant results versus f, where $Y_0 = 1/Z_0$. At the beginning, this parameter with the only real part seems to go up and then down to zero as a sinusoidal function of f. As f increases into the bandgap, its real quantity is converted to its imaginary counterpart, and then varies up and down to zero again. Equation (4) yields that Y_0 must be real at the low range since there exists the only real term, i.e., $\sin(\beta T)$, at the right-hand side due to $\alpha = 0$. Within the bandstop, the only

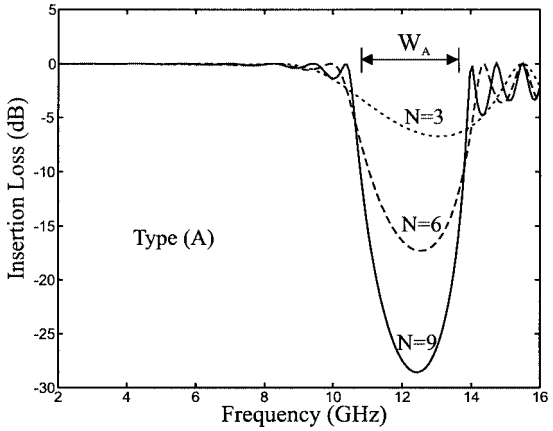

(a)

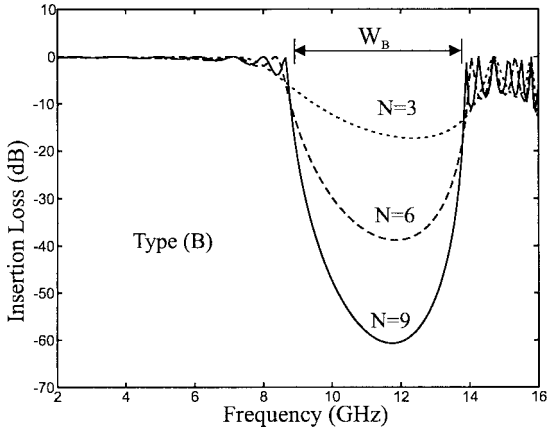

(b)

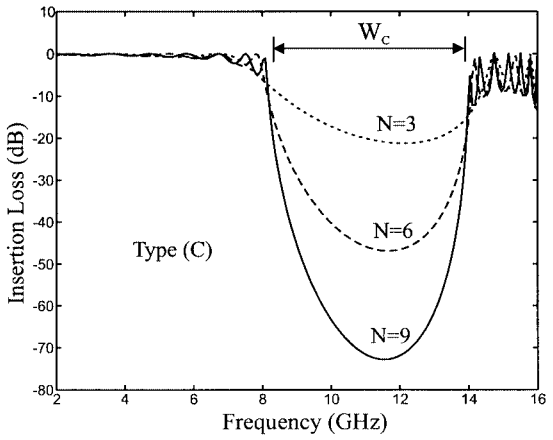

(c)

Fig. 7. Simulated insertion loss (S_{21}) of three types of periodic CPW structures with finite cells of $N = 3, 6,$ and 9 via extracted unit-length transmission parameters. (a) Type (A). (b) Type (B). (c) Type (C).

imaginary term can remain at the right-hand side, i.e., $-j(e^{\alpha T} - e^{-\alpha T})/2$, due to nonzero α and $\beta T = \pi$ Thereby, Y_0 or Z_0 must become imaginary as exhibited in Figs. 3(c), 4(c), and 5(c) as follows:

$$-jY_0B_p = \frac{e^{\alpha T} + e^{-\alpha T}}{2}\sin(\beta T) - j\frac{e^{\alpha T} - e^{-\alpha T}}{2}\cos(\beta T). \quad (4)$$

Next, the $ABCD$-matrix parameters of the three periodic CPW circuits with finite cells of $N = 3, 6,$ and 9 are calculated via above-extracted unit-length parameters based on a simple transmission-line equation, i.e., (5). Thus, the relevant S-matrix parameters can be obtained, as illustrated in Fig. 7. As N increases, the insertion loss becomes lower and lower so as to realize the deep rejection band, as addressed in many literatures (e.g., [10]). With reference to Figs. 3–5, we can well figure out that the rejection bandwidth in the S-matrix is actually dominated by the above-exhibited bandstop with nonzero α, but it becomes a little wider due to extremely high or low Z_0 outside the bandstop with respect to that of its two feeding lines as follows:

$$\begin{bmatrix} A_N & B_N \\ C_N & D_N \end{bmatrix} = \begin{bmatrix} \cosh(\gamma NT) & Z_0\sinh(\gamma NT) \\ Y_0\sinh(\gamma NT) & \cosh(\gamma NT) \end{bmatrix}. \quad (5)$$

Finally, full-wave simulation via a Momentum simulator is carried out on the overall layout for the three six-cell periodic CPW circuits and, additionally, the three CPW circuit samples are fabricated, as shown in Fig. 8(a). Fig. 8(b) illustrates the comparison among three curves of insertion loss, which are derived from the above-extracted transmission parameters, Momentum simulation, and RF measurement, respectively, giving a good evident validation. Some discrepancies between predicted

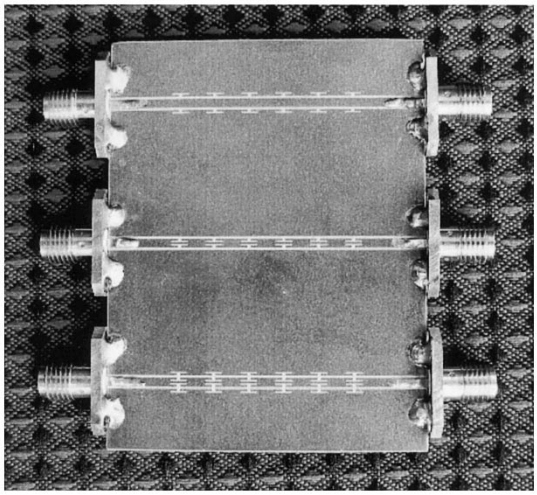

(a)

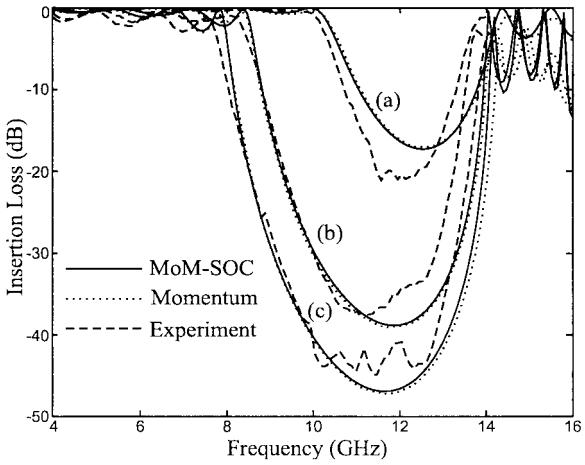

(b)

Fig. 8. Photographic layouts and comparison among the predicted and measured results of the three periodic CPW circuit blocks with the finite cells of $N = 6$. (a) Photograph of three samples. (b) Predicted and measured results.

and measured results may be caused by unexpected tolerance in fabrication and coax-to-CPW transition effects.

IV. Conclusions

In this paper, complex unit-length transmission parameters of periodic CPW structures with inductive loading have been extensively characterized using the full-wave MoM–SOC technique. Extracted propagation constant and characteristic impedance quantitatively have exhibited complete guided-wave characteristics of these periodic structures, i.e., frequency-dependent slow-wave and bandstop behaviors. In particular, for the first time, it has been demonstrated that, within the bandstop, the propagation constant must become complex with a nonzero attenuation constant, while the characteristic impedance must appear purely imaginary. Along with physical explanation, the three six-cell periodic CPW circuits have been designed, fabricated, and measured to give an evident validation in theory and experiment.

Acknowledgment

The author is grateful to H. Shi for her support in the Momentum simulation and experiment.

References

[1] Y. Qian, V. Radisic, and T. Itoh, "Simulation and experiment of photonic band-gap structures for microstrip circuits," in *Asia–Pacific Microwave Conf. Dig.*, Hong Kong, Dec. 1997, pp. 585–588.

[2] F. R. Yang, R. Coccioli, Y. Qian, and T. Itoh, "Planar PBG structures: Basic properties and applications," *IEICE Trans. Electron.*, vol. E83-C, no. 5, pp. 687–696, May 2000.

[3] A. A. Oliner, "Periodic structures and photonic-band-gap terminology: Historical perspective," in *Proc. 29th Eur. Microwave Conf.*, Munich, Germany, Oct. 1999, pp. 295–298.

[4] M. Harris, "Summary on preferred terminology to replace 'photonic bandgap' in describing microwave and millimeter wave periodic structures," *IEEE Microwave Mag.*, vol. 3, p. 75, Sept. 2002.

[5] R. E. Collin, "Periodic structure and filters," in *Foundations for Microwave Engineering*, 2nd ed. New York: McGraw-Hill, 1992, ch. 8.

[6] F. J. Glandorf and I. Wolff, "A spectral-domain analysis of periodically nonuniform microstrip line," *IEEE Trans. Microwave Theory Tech.*, vol. MTT-35, pp. 336–343, Mar. 1987.

[7] H.-Y. D. Yang, "Theory of microstrip lines on artificial periodic substrates," *IEEE Trans. Microwave Theory Tech.*, vol. 47, pp. 629–635, May 1999.

[8] M. Kahrizi, T. K. Sarkar, and Z. A. Maricevic, "Dynamic analysis of a microstrip line over a perforated ground plane," *IEEE Trans. Microwave Theory Tech.*, vol. 42, pp. 820–825, May 1994.

[9] C. K. Wu, H. S. Wu, and C. K. Tzuang, "Electric-magnetic-electric slow-wave microstrip line and bandpass filter of compressed size," *IEEE Trans. Microwave Theory Tech.*, vol. 50, pp. 1996–2004, Aug. 2002.

[10] L. Zhu and K. Wu, "Unified equivalent circuit model of planar discontinuities suitable for field theory-based CAD and optimization of M(H)MICs," *IEEE Trans. Microwave Theory Tech.*, vol. 47, pp. 1589–1602, Sept. 1999.

[11] ——, "Short-open calibration technique for field theory-based parameter extraction of lumped-elements of planar integrated circuits," *IEEE Trans. Microwave Theory Tech.*, vol. 50, pp. 1861–1869, Aug. 2002.

[12] ——, "Revisiting characteristic impedance and its definition of microstrip line with a self-calibration 3-D MoM scheme," *IEEE Microwave Guided Wave Lett.*, vol. 8, pp. 87–89, Feb. 1998.

[13] J. C. Rautio, "Comments on 'Revisiting characteristic impedance and its definition of microstrip line with a self-calibration 3-D MoM scheme'," *IEEE Trans. Microwave Theory Tech.*, vol. 47, pp. 115–117, Jan. 1999.

[14] L. Zhu and K. Wu, "Authors' reply," *IEEE Trans. Microwave Theory Tech.*, vol. 47, pp. 117–119, Jan. 1999.

[15] L. Zhu, "Unified 3-D definition of CPW- and CSL-mode characteristic impedances of coplanar waveguide using MoM–SOC technique," *IEEE Microwave Wireless Comp. Lett.*, vol. 13, pp. 158–160, Apr. 2003.

[16] A. Gorur, G. Karpus, and M. Alkan, "Characteristics of periodically loaded CPW structure," *IEEE Microwave Guided Wave Lett.*, vol. 8, pp. 278–280, Aug. 1998.

[17] J. Sor, Y. Qian, and T. Itoh, "Miniature low-loss CPW periodic structures for filter applications," *IEEE Trans. Microwave Theory Tech.*, vol. 49, pp. 2336–2341, Dec. 2001.

[18] L. Zhu, "Realistic equivalent circuit model of coplanar waveguide open circuit: Lossy shunt resonator network," *IEEE Microwave Wireless Comp. Lett.*, vol. 12, pp. 175–177, May 2002.

[19] L. Zhu and K. Wu, "Model-based characterization of finite-periodic finite-ground coplanar waveguides," in *Proc. Asia–Pacific Microwave Conf.*, Singapore, Nov./Dec. 1999, pp. 112–115.

Lei Zhu (S'91–M'93–SM'00) was born in Wuxi, Jiangsu Province, China, in June 1963. He received the B.Eng. and M.Eng. degrees in radio engineering from the Nanjing Institute of Technology (now Southeast University), Nanjing, China, in 1985 and 1988, respectively, and the Ph.D. Eng. degree in electronic engineering from the University of Electro-Communications, Tokyo, Japan, in 1993.

From 1985 to 1989, he studied a variety of millimeter-wave passive and active circuits, and leaky-wave antennas using the grooved nonradiative dielectric waveguide (GNRD). From 1989 to 1993, he conducted research on the full-wave characterization and optimization design of planar integrated transmission lines and components. From 1993 to 1996, he was a Research Engineer with Matsushita-Kotobuki Electronics Industries Ltd., Tokyo, Japan, where he undertook research and development in the development of planar integrated antenna elements and arrays with compact-size and high radiation gain/efficiency for application in wireless communications. From 1996 to 2000, he was a Research Fellow with the Ecole Polytechnique de Montréal, Montréal, QC, Canada. Since July 2000, he has been an Associate Professor with the School of Electrical and Electronic Engineering, Nanyang Technological University, Singapore. His current research works/interests include the study of planar integrated dual-mode filters, ultra-broad bandpass filters, broad-band interconnects, planar antenna elements/arrays, uniplanar CPW/coplaner stripline (CPS) circuits, as well as full-wave 3-D MoM modeling of planar integrated circuits and antennas, numerical deembedding or parameter-extraction techniques, and field-theory-based computer-aided design (CAD) synthesis/optimization design procedures. He is an Associate Editor for the *IEICE Transactions on Electronics*.

Dr. Zhu is currently a member of the Editorial Board of the IEEE Transactions on Microwave Theory and Techniques. He was the recipient of the Japanese Government (Monbusho) Graduate Fellowship (1989–1993). He was also the recipient of the 1993 First-Order Achievement Award in Science and Technology presented by the National Education Committee, China, the 1996 Silver Award of Excellent Invention presented by the Matsushita-Kotobuki Electronics Industries Ltd., Japan, the 1997 Asia–Pacific Microwave Prize Award presented at the Asia–Pacific Microwave Conference, Hong Kong, and the 2002 Japan Society for the Promotion of Science (JSPS) Invitation Fellowship for Research in Japan from the Japan Society for the Promotion of Science.